Exchange interactions and itinerant ferromagnetism in ultracold Fermi gases

Enya Vermeyen*
TQC, Universiteit Antwerpen, B-2610 Antwerpen, Belgium

Carlos A. R. Sá de Melo
School of Physics, Georgia Institute of Technology, Atlanta, Georgia 30332, USA

Jacques Tempere
TQC, Universiteit Antwerpen, B-2610 Antwerpen, Belgium
and Lyman Laboratory of Physics, Harvard University, Cambridge, Massachusetts 02138, USA

(Received 8 December 2017; revised manuscript received 10 July 2018; published 31 August 2018)

In the 1930s, two main paradigms for the theoretical description of ferromagnetism were developed: Heisenberg ferromagnetism of localized fermions (e.g., in a lattice), and Bloch or Stoner ferromagnetism of nonlocalized fermions (i.e., in a gas), also called itinerant ferromagnetism. Despite many theoretical predictions, itinerant ferromagnetism has remained elusive in experiments. This ferromagnetic state is predicted to occur for strong repulsive interactions, corresponding to a regime that is very challenging to describe theoretically because there are multiple competing physical effects, including superfluid pairing. In this paper, we point out that the problem of itinerant ferromagnetism for atomic Fermi gases is different from that of electron gases in metals due to the short-range nature of the interatomic interactions. We also show that the standard saddle point used to describe itinerant ferromagnetism of the electron gas in metals does not apply, because in the short-range limit of this approximation the Pauli exclusion principle is violated. As a remedy, we introduce a modified interaction pseudopotential for ultracold gases which includes both local (Hartree) and nonlocal (Fock) terms while preserving the Pauli exclusion principle in the short-range regime. Furthermore, we demonstrate the usefulness of this method to study the existence and stability of itinerant ferromagnetism in ultracold atomic gases. Lastly, we obtain the critical temperature for the ferromagnetic transition as a function of the opposite-spin interaction strength and find a rather good agreement with recent experimental results.

DOI: 10.1103/PhysRevA.98.023635

I. INTRODUCTION

In 1929, Bloch suggested that in a system of spin-1/2 fermions, strong repulsive interactions can lead to spontaneous spin polarization, even though the interaction potential is spin independent [1], overcoming the cost in kinetic energy for the Fermi system. This phenomenon is called itinerant ferromagnetism, in contrast to the "localized" or Heisenberg ferromagnetism arising from spins on a lattice [2]. The original context of Bloch's work was electrons in a metal, where the (bare) Coulomb interactions between the electrons are long ranged. Using Wick's theorem, the interaction between a fermion of spin state σ_1 and a fermion of spin state σ_2 can be decoupled as follows:

$$\left\langle \psi^\dagger_{\sigma_1}(\mathbf{r})\psi^\dagger_{\sigma_2}(\mathbf{r}')\psi_{\sigma_2}(\mathbf{r}')\psi_{\sigma_1}(\mathbf{r})\right\rangle \simeq \underbrace{\left\langle \psi^\dagger_{\sigma_1}(\mathbf{r})\psi_{\sigma_1}(\mathbf{r})\right\rangle\left\langle \psi^\dagger_{\sigma_2}(\mathbf{r}')\psi_{\sigma_2}(\mathbf{r}')\right\rangle}_{\text{Hartree}} - \underbrace{\left\langle \psi^\dagger_{\sigma_1}(\mathbf{r})\psi_{\sigma_2}(\mathbf{r}')\right\rangle\left\langle \psi^\dagger_{\sigma_2}(\mathbf{r}')\psi_{\sigma_1}(\mathbf{r})\right\rangle}_{\text{Fock}}. \quad (1)$$

The contribution of the direct (Hartree) interaction is canceled by the positive "jellium" background, and it is the energy lowering that occurs through the exchange (Fock) interaction that drives the spin polarization. By including band and finite temperature effects, Stoner extended Bloch's results [3]. However, subsequent theoretical work by Wigner [4] has revealed that correlation effects beyond Hartree-Fock can suppress the ferromagnetic instability. Moreover, Monte Carlo simulations [5] found a polarized electron liquid only close to the Wigner crystal phase. The instabilities that do survive after correlations are taken into account are charge and spin density waves [6] and also phase separation. It is well known that charge-density wave (CDW) and spin-density wave (SDW) instabilities do not occur in three-dimensional (3D) systems with spherical Fermi surfaces because nesting is suppressed, given that there are no flat regions on the Fermi surface that can be connected by a single nesting vector [7]. However, in one and two dimensions, or in 3D systems with deformed Fermi surfaces that allow for nesting, CDW and SDW are important competing instabilities to the formation of domains. Hence, there is no indication of itinerant ferromagnetism in jellium models at this level of approximation. Indeed, pure itinerant ferromagnetism has not yet been found in solids.

Ultracold atomic gases have been proposed as an alternative model system for the realization of pure itinerant ferromagnetism [8–12]. Using Feshbach resonances the interaction

*Present address: Institute of Astronomy, Catholic University of Leuven, B-3001 Leuven, Belgium; enya.vermeyen@kuleuven.be

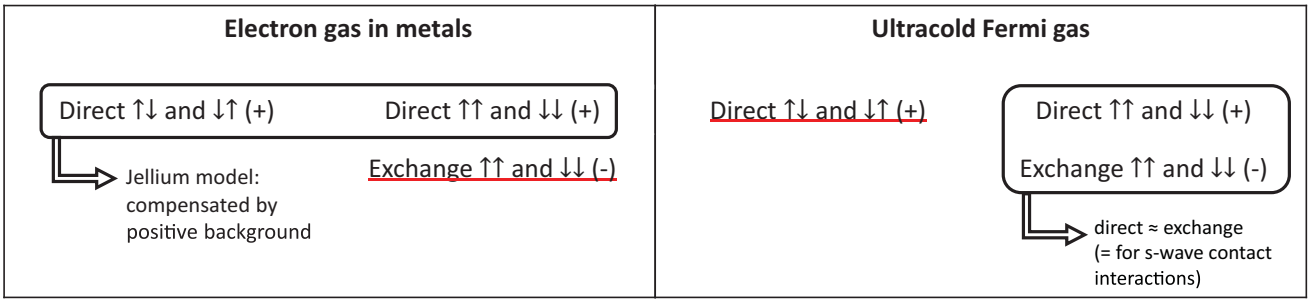

FIG. 1. A comparison of the direct (Hartree) and exchange (Fock) contributions for electrons and ultracold Fermi gases. For free electrons in a material, the total direct interaction energy is compensated by the positive background (jellium model) and only the exchange energy has to be explicitly written. For an ultracold Fermi gas interacting through an s-wave contact potential, the intraspecies direct and exchange interaction energies cancel each other and only the direct interspecies interaction energy has to be written down explicitly. Despite these vastly different expressions for the interaction energy, in both cases the spin polarization is driven by the spin dependency of the exchange interactions. The *total* direct interaction energy remains spin independent as long as the original interaction potential is spin independent.

strength can be tuned, enabling the realization of strong repulsive interactions, where itinerant ferromagnetism is expected to occur. Contrary to Bloch's original context, in neutral atomic gases there is no jellium background and interactions are short ranged. Due to the absence of the jellium background, the direct (Hartree) contribution to the interaction energy is no longer canceled for fermions of opposite spin. In the particular case where the system has only s-wave contact interactions (zero-ranged), the direct contribution is perfectly canceled by the exchange contribution for same-spin fermions (Fig. 1). Indeed, the fermionic antisymmetry requirement does not allow for contact s-wave interactions between same-spin fermions. Nevertheless, spin polarization still reduces the overall interaction energy for repulsive interactions. Whereas in Bloch's context spin polarization causes the exchange energy to become more strongly negative, in the context of quantum gases spin polarization causes the remaining (positive) interspecies direct energy to become smaller. Thus, by increasing the interaction strength, a transition towards a spin-polarized state is theoretically expected also in quantum gases.

The theoretical expectation just described motivated a recent experiment in which Ketterle and co-workers were able to probe the regime where itinerant ferromagnetism is expected in an ultracold gas of lithium-6 atoms [13]. However, fast molecular pairing due to the instability of the repulsive branch of the Feshbach resonance prevented the formation of any equilibrium state (precluding formation of the itinerant ferromagnetic state) [14–18]. In response, there have been many proposals for minimizing the effects of this experimental instability [19–23], including making use of mixtures [24], spin-orbit coupling [25], reduced dimensionality [26,27], and optical lattices [28,29]. However, it still remains to be seen whether the itinerant ferromagnetic state itself is stable [30–34]. This has prompted new experiments [35] to investigate itinerant ferromagnetism by studying the dynamics of spin diffusion between initially prepared spin-polarized domains, as this quantity reveals ferromagnetic correlations even if the itinerant ferromagnetic state itself remains unstable.

The current experiments with ultracold Fermi gases remain in a regime where the interactions are captured by a contact s-wave pseudopotential. However, efforts are underway to probe new interaction potentials, most notably dipolar interactions [36–42], but also p-wave interactions [43,44]. In that case, exchange effects in quantum gases will no longer be limited to suppressing the interaction between same-spin fermions (in contrast to the situation in Fig. 1) and the intraspecies interactions will have to be written down explicitly. Consequently, in our theoretical description it is important to take into account correctly both direct and exchange contributions to the interaction energy coming from equal-spin and opposite-spin scattering. Itinerant ferromagnetism has been studied in the functional integral formalism [45,46], based on the Ward-Takahashi identities, in attempts to clarify the role of electron-magnon interactions on the Stoner instability. Subsequent work [47] within this formalism introduced collective quantum fields corresponding to the spin density to theoretically study the onset of itinerant ferromagnetism in metals.

The use of collective quantum fields, from which an order parameter for the itinerant ferromagnetic state can be deduced, is now the mainstream method to study the electron liquid with functional integrals [48,49]. In the case of ultracold Fermi gases, we show that care must be exercised in analyzing the regime of short-ranged interactions. Since the Fock term is nonlocal, using a strictly zero-ranged interaction potential does not capture its contribution [50]. In contrast to electrons in a metal, this problem is relevant for ultracold Fermi gases since short-ranged potentials are widely used to model interatomic interactions. The main aim of this paper is to propose a limiting procedure that includes the Fock contribution correctly when the interactions become very short ranged.

Possible alternative approaches that do not rely on Hubbard-Stratonovich fields might be applied to describe itinerant ferromagnetism. For example, a variational perturbation method proposed by Kleinert [48,51,52] avoids the use of collective quantum fields in favor of classical collective fields. Another method that does not rely on the Hubbard-Stratonovich transform is a dynamical mean-field theory for lattice calculations [53]. However, as our goal is to point out a difficulty with the often used saddle-point expansion of the effective action following a Hubbard-Stratonovich transform, we focus on correcting the problem within that framework and obtain a phase diagram for the uniform ferromagnetic state.

In this context, the collective quantum field is expanded up to quadratic fluctuations around the field configuration that extremizes the effective action for the collective field. These fluctuations describe the low-energy excitations of the system such as sound and spin waves. Previously [30], we have shown that for a contact potential the extremum of the action functional for the collective quantum fields representing the spin densities is not a minimum but represents an unstable state, invalidating the use of Gaussian fluctuations in the Hubbard-Stratonovich scheme. The present treatment allows us to look at more general potentials with finite-ranged s-wave and p-wave interactions, and we derive the region in interaction parameter space where the instability remains present. In the region(s) where the extremum represents a stable state, we classify the nature of the saddle point as unpolarized, partially polarized, or fully polarized. Furthermore, assuming a uniform (single-domain) ferromagnet, we also describe the ferromagnetic transition temperature versus s-wave scattering length and correlate it to an experimental phase diagram that probes the ferromagnetic phase transition through its domain structure [35].

The remainder of the paper is structured as follows. In Sec. II, we first show that applying a naive saddle-point approximation in the Hubbard-Stratonovich formalism leads to a violation of the Pauli exclusion principle for short-ranged interactions. Still in Sec. II, we propose a remedy for this problem by introducing a modified interaction pseudopotential, which is applied in Sec. III to analyze itinerant ferromagnetism in the context of ultracold atomic gases. Finally, conclusions are drawn in Sec. VI.

II. FORMALISM

In Sec. II A, we first discuss the problems that arise when one combines the Hubbard-Stratonovich transformation with the saddle-point approximation for Fermi gases with short-ranged interactions. In Sec. II B, we provide a remedy in order to describe correctly itinerant ferromagnetism at the saddle point and beyond. In Sec. II C, we use our method at the saddle-point level.

A. The trouble with Hubbard-Stratonovich

To obtain a phase diagram requires the calculation of the thermodynamic grand potential per unit volume $\Omega = -\ln(\mathcal{Z})/\beta V$ of the (pseudo)spin-1/2 Fermi gas, with $\mathcal{Z}$ the partition sum, $\beta = 1/k_B T$ proportional to the inverse temperature, and V the volume. In the path-integral formalism, the grand-canonical partition sum can be calculated by summing over all possible configurations of the fermionic Grassmann fields $\psi_{\uparrow,\mathbf{x},\tau}$ and $\psi_{\downarrow,\mathbf{x},\tau}$ (and their conjugated counterparts $\bar{\psi}_\uparrow$ and $\bar{\psi}_\downarrow$), weighted by the Euclidean action S of each configuration: $\mathcal{Z} = \prod_{\sigma=\uparrow,\downarrow} \int \mathcal{D}\bar{\psi}_\sigma \int \mathcal{D}\psi_\sigma \exp(-S[\bar{\psi},\psi])$. The action of the system (in units $\hbar = 1$, $k_B = 1$, the mass of the particles $m = 1/2$, and the Fermi wave vector $k_F = 1$) is given by

$$S[\bar{\psi},\psi] = \sum_{\sigma_1=\uparrow,\downarrow} \int_0^\beta d\tau \int d\mathbf{x} \left[\bar{\psi}_{\sigma_1,\mathbf{x},\tau} \left(\frac{\partial}{\partial\tau} - \nabla_{\mathbf{x}}^2 - \mu_{\sigma_1} \right) \psi_{\sigma_1,\mathbf{x},\tau} + \sum_{\sigma_2=\uparrow,\downarrow} \int d\mathbf{x}' \frac{g_{\sigma_1\sigma_2}(\Delta\mathbf{x})}{2} \bar{\psi}_{\sigma_1,\mathbf{x},\tau} \psi_{\sigma_1,\mathbf{x},\tau} \bar{\psi}_{\sigma_2,\mathbf{x}',\tau} \psi_{\sigma_2,\mathbf{x}',\tau} \right], \quad (2)$$

with τ the imaginary time, μ_σ the spin-σ chemical potential, $g_{\sigma_1\sigma_2}(\Delta\mathbf{x})$ the interaction potential, and $\Delta\mathbf{x} = \mathbf{x} - \mathbf{x}'$. For symmetry reasons, we will assume $g_{\uparrow\downarrow}(\Delta\mathbf{x}) = g_{\downarrow\uparrow}(-\Delta\mathbf{x})$.

Due to the presence of the interaction term in the action, the path integral cannot be calculated exactly for a general case. Instead, the interaction term is decoupled into several terms quadratic in the fermionic fields by introducing an auxiliary bosonic field through the Hubbard-Stratonovich transformation. To study superfluidity, the quartic product is split into a product of the pairs $\bar{\psi}_{\sigma_1,\mathbf{x},\tau} \bar{\psi}_{\sigma_2,\mathbf{x}',\tau}$ and $\psi_{\sigma_1,\mathbf{x},\tau} \psi_{\sigma_2,\mathbf{x}',\tau}$, the so-called Bogoliubov channel. Here, we keep $\bar{\psi}_{\sigma_1,\mathbf{x},\tau} \psi_{\sigma_1,\mathbf{x},\tau}$ and $\bar{\psi}_{\sigma_2,\mathbf{x}',\tau} \psi_{\sigma_2,\mathbf{x}',\tau}$ as quadratic products together, thus using the Hartree channel. The Hubbard-Stratonovich transformation for this channel is given by

$$\exp\left[-\sum_{\sigma_1,\sigma_2=\uparrow,\downarrow} \int dV \frac{g_{\sigma_1\sigma_2}(\Delta\mathbf{x})}{2} \bar{\psi}_{\sigma_1,\mathbf{x},\tau} \psi_{\sigma_1,\mathbf{x},\tau} \bar{\psi}_{\sigma_2,\mathbf{x}',\tau} \psi_{\sigma_2,\mathbf{x}',\tau} \right]$$
$$= \frac{1}{\mathcal{Z}_\rho} \int \mathcal{D}\rho_\uparrow \int \mathcal{D}\rho_\downarrow \exp\left[\sum_{\sigma_1,\sigma_2=\uparrow,\downarrow} \int dV \frac{g_{\sigma_1\sigma_2}(\Delta\mathbf{x})}{2} \left(\rho_{\sigma_1,\mathbf{x},\tau} \rho_{\sigma_2,\mathbf{x}',\tau} - \rho_{\sigma_1,\mathbf{x},\tau} \bar{\psi}_{\sigma_2,\mathbf{x}',\tau} \psi_{\sigma_2,\mathbf{x}',\tau} - \bar{\psi}_{\sigma_1,\mathbf{x},\tau} \psi_{\sigma_1,\mathbf{x},\tau} \rho_{\sigma_2,\mathbf{x}',\tau} \right) \right], \quad (3)$$

with $\int dV = \int_0^\beta d\tau \int d\mathbf{x} \int d\mathbf{x}'$. In the functional integral identity above, two real-valued collective quantum fields $\rho_\uparrow$ and $\rho_\downarrow$ are introduced as auxiliary variables and are integrated over. The prefactor $\mathcal{Z}_\rho$ shifts the zero point of the thermodynamic grand potential and will be taken as our energy reference. First, notice that even though this decomposition is called the Hartree *channel*, it is an exact relation and thus contains all contributions to the interaction *energy*: Hartree, Fock, and Bogoliubov energy contributions are accounted for through the full functional integration over the quantum fields $\rho_\uparrow$ and $\rho_\downarrow$. Of course, approximations to the full functional integral may lose or neglect some of these contributions. In the Hartree channel, this may lead to a loss of the exchange interactions.

To clarify this point, consider the Grassmann algebra generated by two Grassmann elements $\bar{\psi}_\alpha$ and ψ_α. In the Grassmann-Berezin integral

$$\mathcal{I} = \int \mathcal{D}\psi \exp(\varepsilon_\alpha \bar{\psi}_\alpha \psi_\alpha + g \bar{\psi}_\alpha \psi_\alpha \bar{\psi}_\alpha \psi_\alpha) = \varepsilon_\alpha, \quad (4)$$

where $\int \mathcal{D}\psi = \int d\bar{\psi}_\alpha \int d\psi_\alpha$, it is clear that the quartic term in the exponential does not contribute, since it contains squares of Grassmann variables. Regardless, we can apply the Hubbard-Stratonovich trick to rewrite this quartic part:

$$\exp(g\bar{\psi}_\alpha\psi_\alpha\bar{\psi}_\alpha\psi_\alpha) = \frac{1}{g\pi}\int_{\mathbb{C}} dz\ \exp\left(-\frac{|z|^2}{g} - z\bar{\psi}_\alpha\psi_\alpha - z^*\bar{\psi}_\alpha\psi_\alpha\right). \quad (5)$$

In our simple example, the auxiliary quantum field is reduced to a single complex number z that needs to be integrated over. Substituting this one obtains

$$\mathcal{I} = \frac{1}{g\pi}\int_{\mathbb{C}} dz \exp\left(-\frac{|z|^2}{g}\right) \times \int \mathcal{D}\psi\ \exp(\varepsilon_\alpha\bar{\psi}_\alpha\psi_\alpha - z\bar{\psi}_\alpha\psi_\alpha - z^*\bar{\psi}_\alpha\psi_\alpha). \quad (6)$$

Performing the Grassmann-Berezin integrations first now yields

$$\mathcal{I} = \frac{1}{g\pi}\int_{\mathbb{C}} dz(\varepsilon_\alpha - \mathrm{Re}\,[z])\exp\left(-\frac{|z|^2}{g}\right). \quad (7)$$

As long as the integration over z is performed exactly, the term with $\mathrm{Re}\,[z] = x$ vanishes. However, the saddle-point approximation results in a term

$$\int dx \exp(-x^2/g + \ln(x)) \approx \sqrt{\frac{\pi g}{2}}\, x_{\mathrm{sp}} \exp\left(-x_{\mathrm{sp}}^2/g\right) \quad (8)$$

with $x_{\mathrm{sp}} = \sqrt{g/2}$, so that in this approximation the term $g\bar{\psi}_\alpha\psi_\alpha\bar{\psi}_\alpha\psi_\alpha$ contributes to the energy, violating the exclusion principle.

B. The remedy for the missing exchange

As remarked above, in quantum gases contact interactions $V(\Delta\mathbf{x}) = g\delta(\Delta\mathbf{x})$ do not affect spin-polarized Fermi gases. However, as the simplified example shows, after the Hubbard-Stratonovich transformation, the saddle-point approximation for the density field $\rho_{\mathbf{x}} = \rho_{\mathbf{0}}$ no longer forces the terms with $\Delta\mathbf{x} = \mathbf{0}$ and equal spin to vanish. The decoupling discussed in Eq. (3) has been used to treat the ferromagnetic instability in the electron gas in a solid (see Ref. [49]), where the long-range part of the potential is important, and no major difficulty with the Hartree channel arises. However, for atomic gases, the effective potential is short ranged and the saddle-point approximation in the Hartree channel leads to large inaccuracies, including the violation of the Pauli exclusion principle.

The interaction energy in the Hartree-Fock approximation for a system can be written as

$$E_{\mathrm{HF}} = \frac{1}{2}\sum_{\sigma_1\sigma_2}\int d\mathbf{x}\int d\mathbf{x}' g_{\sigma_1\sigma_2}(\Delta\mathbf{x})\big[\rho_{\sigma_1}(\mathbf{x})\rho_{\sigma_2}(\mathbf{x}') - \zeta_{\sigma_1,\sigma_2}(\mathbf{x},\mathbf{x}')\zeta_{\sigma_2,\sigma_1}(\mathbf{x}',\mathbf{x})\big], \quad (9)$$

where we denote

$$\rho_{\sigma_1}(\mathbf{x}) = \left\langle\psi^\dagger_{\sigma_1}(\mathbf{x})\psi_{\sigma_1}(\mathbf{x})\right\rangle, \quad (10)$$

$$\zeta_{\sigma_1,\sigma_2}(\mathbf{x},\mathbf{x}') = \left\langle\psi^\dagger_{\sigma_1}(\mathbf{x})\psi_{\sigma_2}(\mathbf{x}')\right\rangle. \quad (11)$$

The saddle-point approximation for short-ranged interactions, on the other hand, results in a saddle-point energy

$$E_{\mathrm{sp}} = \frac{1}{2}\sum_{\sigma_1\sigma_2}\int d\mathbf{x}\int d\mathbf{x}' g_{\sigma_1\sigma_2}(\Delta\mathbf{x})\rho_{\sigma_1}(\mathbf{x})\rho_{\sigma_2}(\mathbf{x}'). \quad (12)$$

Now, notice that the Hartree-Fock energy can be rewritten as

$$E_{\mathrm{HF}} = \frac{1}{2}\sum_{\sigma_1\sigma_2}\int d\mathbf{x}\int d\mathbf{x}' \tilde{g}_{\sigma_1\sigma_2}(\Delta\mathbf{x})\rho_{\sigma_1}(\mathbf{x})\rho_{\sigma_2}(\mathbf{x}'), \quad (13)$$

with

$$\tilde{g}_{\sigma_1\sigma_2}(\Delta\mathbf{x}) = g_{\sigma_1\sigma_2}(\Delta\mathbf{x})\left(1 - \frac{\zeta_{\sigma_1,\sigma_2}(\mathbf{x},\mathbf{x}')}{\rho_{\sigma_1}(\mathbf{x})}\frac{\zeta_{\sigma_2,\sigma_1}(\mathbf{x}',\mathbf{x})}{\rho_{\sigma_2}(\mathbf{x}')}\delta_{\sigma_1,\sigma_2}\right), \quad (14)$$

where $\delta_{\sigma_1,\sigma_2}$ is the Kronecker δ. This is obtained by simply dividing and multiplying the Fock term by the product of two densities. Recall that the product $\zeta_{\sigma_1,\sigma_2}(\mathbf{x},\mathbf{x}')\zeta_{\sigma_2,\sigma_1}(\mathbf{x}',\mathbf{x})$ is the result of the Wick decomposition of a two-particle correlator that varies spatially on a scale corresponding to the exchange correlation length ξ_{ex}. This implies that $\zeta_{\sigma,\sigma}(\mathbf{x},\mathbf{x}+\Delta\mathbf{x})$ also goes to zero when $|\Delta\mathbf{x}|/\xi_{\mathrm{ex}} \to \infty$, whereas it is equal to $\rho_\sigma(\mathbf{x})$ when $|\Delta\mathbf{x}|/\xi_{\mathrm{ex}} \to 0$. When the density varies slowly in comparison to ξ_{ex}, then

$$f_\sigma(\Delta\mathbf{x}) := \frac{\zeta_{\sigma,\sigma}(\mathbf{x},\mathbf{x}+\Delta\mathbf{x})}{\rho_\sigma(\mathbf{x})} \quad (15)$$

is independent of $\mathbf{x}$. Moreover, the following limit applies:

$$\lim_{\Delta\mathbf{x}\to 0} f_\sigma(\Delta\mathbf{x}) = 1. \quad (16)$$

However, as $|\Delta\mathbf{x}| \gg \xi_{\mathrm{ex}}$, $f_\sigma(\Delta\mathbf{x})$ decreases to zero. Then, we can model this exchange hole through the effective interaction

$$\tilde{g}_{\sigma_1\sigma_2}(\Delta\mathbf{x}) \approx g_{\sigma_1\sigma_2}(\Delta\mathbf{x})\big[1 - f^2_{\sigma_1}(\Delta\mathbf{x})\delta_{\sigma_1,\sigma_2}\big], \quad (17)$$

where $f^2_\sigma(\Delta\mathbf{x})$ can be interpreted as a "shielding" function, equal to 1 for $\Delta\mathbf{x} = 0$ and which can be set to zero for $|\Delta\mathbf{x}| \gg \xi_{\mathrm{ex}}$. When one uses expression (17) instead of $g_{\sigma_1\sigma_2}(\Delta\mathbf{x})$ in the functional integral formalism, the resulting saddle-point energy expression (12) will be equal to the Hartree-Fock result (13). Hence this provides a way of correctly taking into account the Fock contribution by fixing the problem at $\Delta\mathbf{x} = 0$.

After the Hubbard-Stratonovich transformation, a new effective action is defined, which is Fourier transformed in order to remove the derivatives from the kinetic energy. If $\tilde{g}_{\sigma_1\sigma_2}(\Delta\mathbf{x}) = \tilde{g}_{\sigma_1\sigma_2}(-\Delta\mathbf{x})$, one obtains

$$S_{\mathrm{eff}}[\bar{\psi},\psi,\rho] = \sum_{\sigma_1=\uparrow,\downarrow}\sum_{k,k'}\bar{\psi}_{\sigma_1,k}\big[-G^{-1}_{\sigma_1}(k,k')\big]\psi_{\sigma_1,k'} - \frac{\sqrt{V}}{2}\sum_{\sigma_1,\sigma_2=\uparrow,\downarrow}\sum_{Q}\tilde{g}_{\sigma_1\sigma_2}(\mathbf{Q})\rho_{\sigma_1,-Q}\rho_{\sigma_2,Q}, \quad (18)$$

where $k = (\mathbf{k},\boldsymbol{\omega}_n)$ and $Q = (\mathbf{Q},\Omega_m)$ are four-vectors, ω_n and Ω_m are the fermionic and bosonic Matsubara frequencies, respectively, while

$$-G^{-1}_{\sigma_1}(k,k') = \left(-i\omega_n + \mathbf{k}^2 - \mu_{\sigma_1}\right)\delta(\Delta k) + \frac{1}{\sqrt{\beta}}\sum_{\sigma_2=\uparrow,\downarrow}\tilde{g}_{\sigma_1\sigma_2}(\Delta\mathbf{k})\rho_{\sigma_2,\Delta k} \quad (19)$$

is the inverse Green's function, and $\delta(\Delta k)$ is the Dirac δ function with $\Delta k = k - k'$. After performing the fermionic path integral, the partition sum is given by

$$\mathcal{Z} = \int \mathcal{D}\rho_\uparrow \int \mathcal{D}\rho_\downarrow \exp\left(\sum_{\sigma_1=\uparrow,\downarrow} \mathrm{Tr}\left\{\ln\left[-G_{\sigma_1}^{-1}(k,k')\right]\right\} + \frac{\sqrt{V}}{2} \sum_{\sigma_1,\sigma_2=\uparrow,\downarrow} \sum_{Q} \tilde{g}_{\sigma_1\sigma_2}(\mathbf{Q}) \rho_{\sigma_1,-Q} \rho_{\sigma_2,Q} \right). \quad (20)$$

As we show in the next section, the long-wavelength ($\mathbf{Q} \to 0$) limit of Eq. (20) leads to the preservation of equal-spin correlations. The regularized pseudopotential forces the system to remember that these correlations come from finite-ranged interactions.

C. Saddle-point approximation

The remaining bosonic path integral in Eq. (20) cannot be calculated exactly for a general case. In the saddle-point approximation, the densities are assumed to be constant: $\rho_{\sigma,Q} = \sqrt{\beta V}\delta(Q)\rho_\sigma$. This results in the following expression for the saddle-point thermodynamic grand potential as a function of $(\beta, \mu_\uparrow, \mu_\downarrow; \rho_\uparrow, \rho_\downarrow)$ in D dimensions:

$$\Omega_{\mathrm{sp}} = -\frac{1}{2} \sum_{\sigma_1,\sigma_2=\uparrow,\downarrow} \tilde{g}_{\sigma_1\sigma_2} \rho_{\sigma_1} \rho_{\sigma_2} + \Omega_{\mathrm{sp,kin}}(\beta, \mu'_\uparrow, \mu'_\downarrow), \quad (21)$$

where we defined new interaction parameters

$$\tilde{g}_{\sigma_1\sigma_2} = \sqrt{V}\,\tilde{g}_{\sigma_1\sigma_2}(\mathbf{Q}=\mathbf{0}) = \int_V d(\Delta\mathbf{x}) \tilde{g}_{\sigma_1\sigma_2}(\Delta\mathbf{x}) \quad (22)$$

and an effective chemical potential

$$\mu'_{\sigma_1} = \mu_{\sigma_1} - \sum_{\sigma_2=\uparrow,\downarrow} \tilde{g}_{\sigma_1\sigma_2} \rho_{\sigma_2}. \quad (23)$$

We would like to emphasize that both the bare $g_{\sigma_1\sigma_2}(\Delta\mathbf{x})$ and the renormalized $\tilde{g}_{\sigma_1\sigma_2}(\Delta\mathbf{x})$ interactions for equal spins as well as opposite spins are assumed to have a finite range from the onset. As can be seen from Eq. (22), the interaction parameters $\tilde{g}_{\sigma_1\sigma_2}$ are spatial averages and depend on the interaction range. It is only in the later sections, when we perform a comparison with experiments, that we take the s-wave interaction between opposite spins to have zero range (with scattering length a_s), and the p-wave interaction between equal spins to have spatial range $r_p > 0$ (with scattering volume a_p). The first term in Eq. (21) represents the interaction energy, while the second one represents the kinetic energy,

$$\Omega_{\mathrm{sp,kin}}(\beta, \mu'_\uparrow, \mu'_\downarrow) = \sum_{\sigma_1=\uparrow,\downarrow} \int \frac{d^D k}{(2\pi)^D} \left(\mathbf{k}^2 - \mu'_{\sigma_1} - \frac{1}{\beta} \ln\left\{1 + \exp\left[\beta\left(\mathbf{k}^2 - \mu'_{\sigma_1}\right)\right]\right\} \right). \quad (24)$$

It has the same form as the kinetic energy of the noninteracting gas, but its chemical potentials are shifted by the interactions.

In Eqs. (21) and (23), the values of $\rho_\uparrow$ and $\rho_\downarrow$ are determined using the saddle-point equations,

$$\left.\frac{\partial \Omega_{\mathrm{sp}}(\beta, \mu_\uparrow, \mu_\downarrow; \rho_\uparrow, \rho_\downarrow)}{\partial \rho_\sigma}\right|_{\beta,\mu_\uparrow,\mu_\downarrow;\rho_{-\sigma}} = 0, \quad (25)$$

while the particle number density of each spin state σ is given by the number equations

$$n_\sigma = -\left.\frac{\partial \Omega_{\mathrm{sp}}(\beta, \mu_\uparrow, \mu_\downarrow)}{\partial \mu_\sigma}\right|_{\beta,\mu_{-\sigma}}. \quad (26)$$

The saddle-point condition defined in Eq. (25) can be used to find a spin-dependent uniform density solution $\rho_\sigma = n_\sigma$. From these results, we obtain next the polarization $P = (n_\uparrow - n_\downarrow)/(n_\uparrow + n_\downarrow)$ as a function of interaction strength and temperature to characterize the regions of phase space where itinerant ferromagnetism emerges.

III. HESSIAN MATRIX AT THE SADDLE POINT

A solution to the saddle-point equations (hereafter called a saddle point) is physical only if it is also a minimum of the saddle-point thermodynamic grand potential Ω_{sp} as a function of $\rho_\uparrow$ and $\rho_\downarrow$. If it is not a minimum, it is unstable to (uniform) density fluctuations. The stability of saddle-point solutions can be tested by studying its Hessian matrix H of second derivatives of Ω_{sp} with respect to $\rho_\uparrow$ and $\rho_\downarrow$. If H has two positive eigenvalues, that is, if both its trace and determinant are positive, a saddle point is also a minimum and thus stable against (uniform) density fluctuations. In this section, we derive the stability conditions and the corresponding polarization of saddle-point solutions for the particular example of exchange-induced itinerant ferromagnetism in three dimensions. We also obtain the temperature versus interaction phase diagram for a uniform (single-domain) ferromagnetic state.

In order to exclude other sources of polarization, we limit ourselves to the case $\tilde{g}_{\downarrow\downarrow} = \tilde{g}_{\uparrow\uparrow} = \tilde{g}_{\mathrm{eq}}$ and use units such that $k_F = (3\pi^2 n)^{3/2}$ (with $n = n_\uparrow + n_\downarrow$) is equal to 1. This means that the saddle-point equations have to be solved in conjunction with the equation for the chemical potential μ that fixes the total density to $n = 1/3\pi^2$. Hence, the parameter space for the phase diagrams are the intraspecies interaction strength $\tilde{g}_{\mathrm{eq}}$, the interspecies interaction strength $\tilde{g}_{\uparrow\downarrow}$, and the inverse temperature β. Note that the chosen example represents a *uniform* system in the *grand-canonical ensemble*, which is different from the case of ultracold atoms confined in a trap, where the number of particles is fixed, the density is inhomogeneous, and itinerant ferromagnetism is exhibited through phase separation in magnetic domains. Our description is more suitable for a system of cold atoms in a box potential, where uniform and single-domain ferromagnetic solutions may arise.

For a given polarization P and inverse temperature β, the remaining number and the saddle-point equations are used to calculate the effective chemical potentials $\mu'_\uparrow$ and $\mu'_\downarrow$, which differ from the actual chemical potentials $\mu_\uparrow$ and $\mu_\downarrow$ as shown in Eq. (23). When these values are substituted in

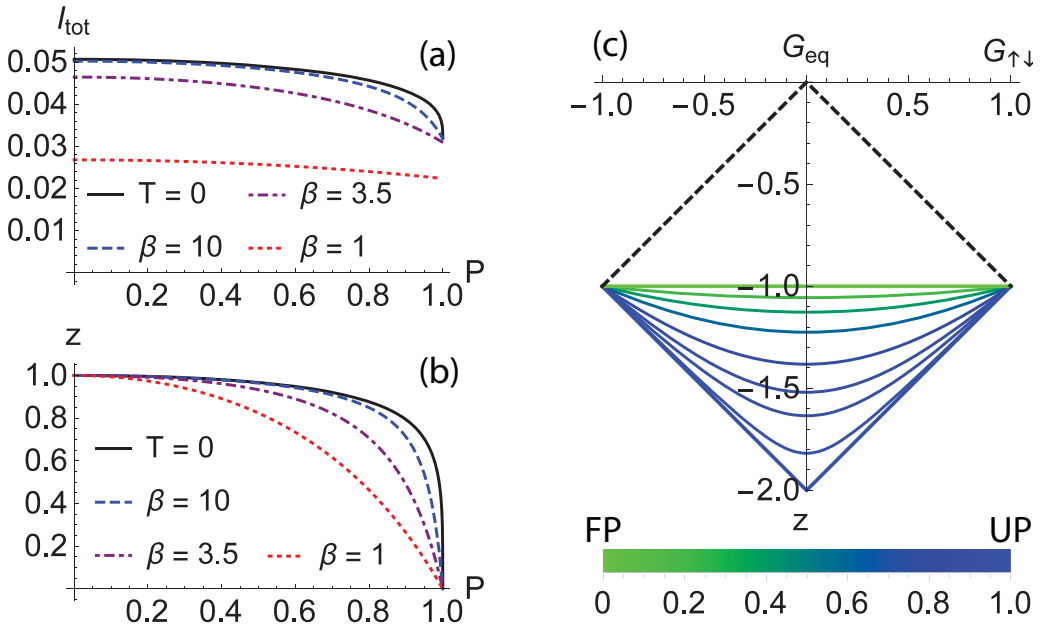

FIG. 2. (a, b) The parameters I_{tot} (a) and z (b) as a function of the polarization P for different values of the inverse temperature: $\beta \to +\infty$ ($T = 0$, black solid line), $\beta = 10$ (blue dashed line), $\beta = 3.5$ (purple dot-dashed line), and $\beta = 1$ (red dotted line). (c) The regions where the Hessian is positive definite are shown for different values of z as a function of the scaled interaction parameters $G_{\uparrow\downarrow} = I_{tot}\tilde{g}_{\uparrow\downarrow}$ and $G_{eq} = I_{tot}\tilde{g}_{eq}$. The black dashed line is the upper boundary (independent of z), while the colored solid lines (for different values of z) are the lower boundaries of the regions where the Hessian is positive definite.

$\Omega_{sp}(\beta, \mu_\uparrow, \mu_\downarrow; n_\uparrow, n_\downarrow)$, the Hessian matrix becomes

$$H = -\begin{pmatrix} \tilde{g}_{\uparrow\uparrow} & \tilde{g}_{\uparrow\downarrow} \\ \tilde{g}_{\uparrow\downarrow} & \tilde{g}_{\downarrow\downarrow} \end{pmatrix} - \begin{pmatrix} \tilde{g}_{\uparrow\uparrow}^2 I_\uparrow + \tilde{g}_{\uparrow\downarrow}^2 I_\downarrow & \tilde{g}_{\uparrow\downarrow}(\tilde{g}_{\uparrow\uparrow} I_\uparrow + \tilde{g}_{\downarrow\downarrow} I_\downarrow) \\ \tilde{g}_{\uparrow\downarrow}(\tilde{g}_{\uparrow\uparrow} I_\uparrow + \tilde{g}_{\downarrow\downarrow} I_\downarrow) & \tilde{g}_{\uparrow\downarrow}^2 I_\uparrow + \tilde{g}_{\downarrow\downarrow}^2 I_\downarrow \end{pmatrix}, \quad (27)$$

where the positive functions $I_\uparrow$ and $I_\downarrow$ are given by

$$I_\sigma(\beta, \mu'_\sigma) = -\left.\frac{\partial^2 \Omega_{sp,kin}}{(\partial \mu'_\sigma)^2}\right|_{\beta, \mu'_{-\sigma}} = \frac{\beta}{2}\int \frac{d^D k}{(2\pi)^D}\left\{\frac{1}{1 + \cosh[\beta(\mathbf{k}^2 - \mu'_\sigma)]}\right\}. \quad (28)$$

Subsequently, the conditions $\mathrm{Tr}\, H \geqslant 0$ and $\det H \geqslant 0$ are used to derive the stability condition, which can be written in terms of the rescaled interaction parameters $G_{eq} = I_{tot}\tilde{g}_{eq}$ and $G_{\uparrow\downarrow} = I_{tot}\tilde{g}_{\uparrow\downarrow}$ (with $I_{tot} = I_\uparrow + I_\downarrow$) as

$$-|G_{\uparrow\downarrow}| \geqslant G_{eq} \geqslant -\frac{2}{z} + \sqrt{\frac{4(1-z)}{z^2} + G_{\uparrow\downarrow}^2}, \quad (29)$$

with $z = 4I_\uparrow I_\downarrow / I_{tot}^2 \in [0, 1]$.

The functions I_{tot} and z decrease monotonously with increasing polarization and temperature, as shown in Figs. 2(a) and 2(b). While the scaling function I_{tot} determines the size of the stability region in the original interaction parameter space, the parameter z determines the shape of the stability area [see Fig. 2(c)]. The value of z is strongly tied to the polarization of the saddle points: $z = 1$ for $P = 0$ and $z = 0$ for $P = 1$. However, for intermediate polarizations, z still depends on the inverse temperature β as shown in Fig. 2(b).

Within the stability region defined by Eq. (29) and shown in Fig. 2(c), solutions to the saddle-point equations are minimal and thus stable, *provided that they exist*. So far, we have presumed that a solution with a particular polarization P exists at a specific inverse temperature β and we calculated the corresponding effective chemical potentials μ'_σ. However, the corresponding value of the chemical potential μ_σ still needs to be calculated from Eq. (23), which defines the effective chemical potential. If no value of μ_σ can be found that satisfies Eq. (23), no saddle points exist for the chosen values of β, P, $g_{\uparrow\downarrow}$, and g_{eq}. As a next step in our calculation, we establish the existence conditions of the saddle-point solutions regardless of their stability. These existence conditions are divided in three categories, depending on the polarization of the corresponding saddle points: unpolarized (UP), partially polarized (PP), and fully polarized (FP). Finally, the stability and existence conditions are combined to produce stability-existence phase diagrams.

For the UP saddle points ($P = 0$), Eq. (23) becomes $\mu' = \mu - \tilde{g}_{eq}/6\pi^2$ and a valid solution can always be found by adapting μ. Consequently, unpolarized saddle points exist for all values of the inverse temperature β and in all parts of the $(g_{\uparrow\downarrow}, g_{eq})$ plane. This implies that the unpolarized stability region is equal to its stability-existence region.

For the partially polarized (PP) solutions ($0 < |P| < 1$), Eq. (23) corresponds to a system of two equations that can be rewritten into the existence condition $G_{eq} = G_{\uparrow\downarrow} - 6\pi^2 \zeta' I_{tot}/P$, with $\zeta' = (\mu'_\uparrow - \mu'_\downarrow)/2$ being equal to half of the effective chemical potential difference. This represents a straight line in the $(G_{\uparrow\downarrow}, G_{eq})$ plane, which may intersect the corresponding stability area if the condition $0 \leqslant 3\pi^2 \zeta' I_{tot}/P \leqslant 1$ is satisfied. The parameter $3\pi^2 \zeta' I_{tot}/P$ has a physical meaning: it can be rewritten as the ratio χ_{diff}/χ_{tot}

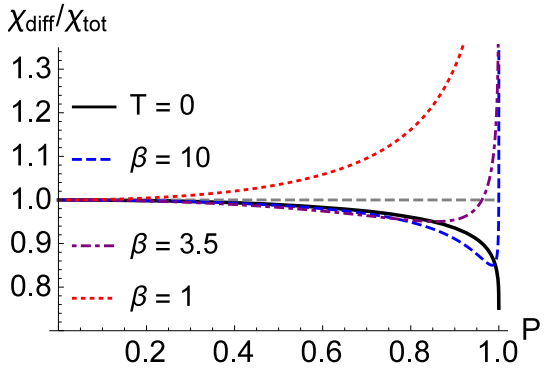

FIG. 3. The ratio $\chi_{\rm diff}/\chi_{\rm tot}$ between the differential and total susceptibility as a function of the polarization P for different values of the inverse temperature: $\beta \to +\infty$ ($T = 0$, black solid line), $\beta = 10$ (blue dashed line), $\beta = 3.5$ (purple dot-dashed line), and $\beta = 1$ (red dotted line).

between the differential susceptibility $\chi_{\rm diff} = \partial(\delta n)/\partial\zeta'|_{\beta,\mu'} = I_{\rm tot}$ and the total susceptibility $\chi_{\rm tot} = \delta n/\zeta'$, where $\delta n = n_\uparrow - n_\downarrow$. These quantities are defined in analogy to their magnetic counterparts. In Fig. 3, $\chi_{\rm diff}/\chi_{\rm tot}$ is shown for different values of β. For finite values of β, $\chi_{\rm diff}/\chi_{\rm tot} \to +\infty$ if $P \to 1$. At low temperatures, PP saddle points can only be stable up to a maximum polarization $P_{\rm max}$, which decreases as a function of temperature as shown in Fig. 4. For $\beta \lesssim 1.715$, none of the PP saddle points are stable.

Fully polarized (FP) saddle points only exist at zero temperature, because $n_\sigma = 0$ can only be achieved in the limit $\mu_\sigma \to +\infty$ at nonzero temperatures. This is an important qualitative difference between zero and nonzero temperatures. At zero temperature, FP solutions to the number equations exist for $\zeta' \geqslant 2^{-1/3}$. For the PP solutions, only one value of ζ' corresponds to each value of P, and the resulting existence condition represents a straight line in the $(G_{\uparrow\downarrow}, G_{\rm eq})$ plane. For the FP solutions at zero temperature, each possible value of ζ' corresponds to a similar existence condition in the form of a straight line in the $(G_{\uparrow\downarrow}, G_{\rm eq})$ plane. This infinite collection of

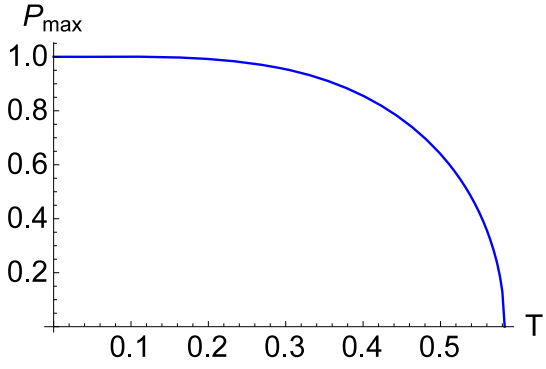

FIG. 4. The maximum value $P_{\rm max}$ of the polarization P for which PP (and FP) saddle points can be stable as a function of the temperature $T = 1/\beta$. Polarized saddle points can only be stable for $T \gtrsim 0.583$ (or $\beta \lesssim 1.715$).

straight lines forms an existence plane defined by the condition $G_{\rm eq} \leqslant G_{\uparrow\downarrow} - 3\pi^2 2^{2/3} I_{\rm tot}$.

By combining the existence and stability conditions, we obtain finite temperature phase diagrams as a function of the modified interaction parameters $\tilde{g}_{\rm eq}$ and $\tilde{g}_{\uparrow\downarrow}$ as shown in Fig. 5. Stable saddle points are only found in the lowest quadrant ($\tilde{g}_{\rm eq} \leqslant |\tilde{g}_{\uparrow\downarrow}|$). The UP stability region is a square which increases in size as a function of temperature. The FP and PP stability regions shrink and become less polarized as a function of temperature, until they are completely absorbed by the growing UP area. If $|\tilde{g}_{\rm eq}|$ or $|\tilde{g}_{\uparrow\downarrow}|$ are too large, the system is susceptible to density fluctuations and none of the saddle points is stable. This greatly reduces the itinerant ferromagnetic (PP and FP) areas in the phase diagram, which may explain why itinerant ferromagnetism is so notoriously hard to find experimentally.

IV. CONNECTION TO EXPERIMENT

The results shown in Fig. 5 can be related to experiments in ultracold atomic gases using $\tilde{g}_{\uparrow\downarrow} = 8\pi k_F a_s$, where a_s is the s-wave scattering length. The parameter $\tilde{g}_{\rm eq}$ describes the strength of the equal-spin correlations and can be estimated as $\tilde{g}_{\rm eq} = -8\pi k_F a_p / r_p^2$, where a_p is the p-wave scattering volume and r_p is the spatial interaction range. Here, we set $\tilde{g}_{\rm eq} = -31$, close to the largest negative value it can take for the ferromagnetic state to be stable. Then we track the existence-stability range of $\tilde{g}_{\uparrow\downarrow}$ as a function of temperature for the combined FP and PP phases.

In Fig. 6, we show the resulting critical temperature as a function of $k_F a_s$ as black dots connected by solid black curves. There is a critical interaction strength above which the saddle-point solution is no longer stable, as indicated by the black dash-dotted line. We defer the discussion of the upper critical interaction strength to the next section and first compare the results below that value to experimental results. The red squares are experimental results [35] and the red dashed curve is a square-root fit also discussed in that work. We find that the minimum interaction strength for the onset of ferromagnetism is $k_F a_s = 0.65$. In experiments [35], the value $k_F a_s = 0.8$ was obtained, in agreement with Monte Carlo simulations [54]. Both values are substantially smaller than that of the Stoner criterion $k_F a_s = \pi/2$, even when second-order corrections [12] lower the value of $k_F a_s$ from $\pi/2$ to 1.05. Given that the present theory does not take into account fluctuations, which tend to lower the critical temperature and increase the critical $k_F a_s$ value, the qualitative agreement with the experimental data is rather good.

Note that the experiment corresponds to an essentially nonequilibrium measurement, from which equilibrium properties are inferred. In the experiment [35], there are two types of metastability involved: metastability with respect to spin diffusion, and metastability associated with staying on the upper energy branch of the scattering states. Itinerant ferromagnetism occurs only in the upper branch, so it is intrinsically limited in lifetime by the decay to the lower branch due to inelastic collisions [35]. In our work, we do not consider this type of decay, that is, we assume that the scattering states in the upper branch have infinite lifetime.

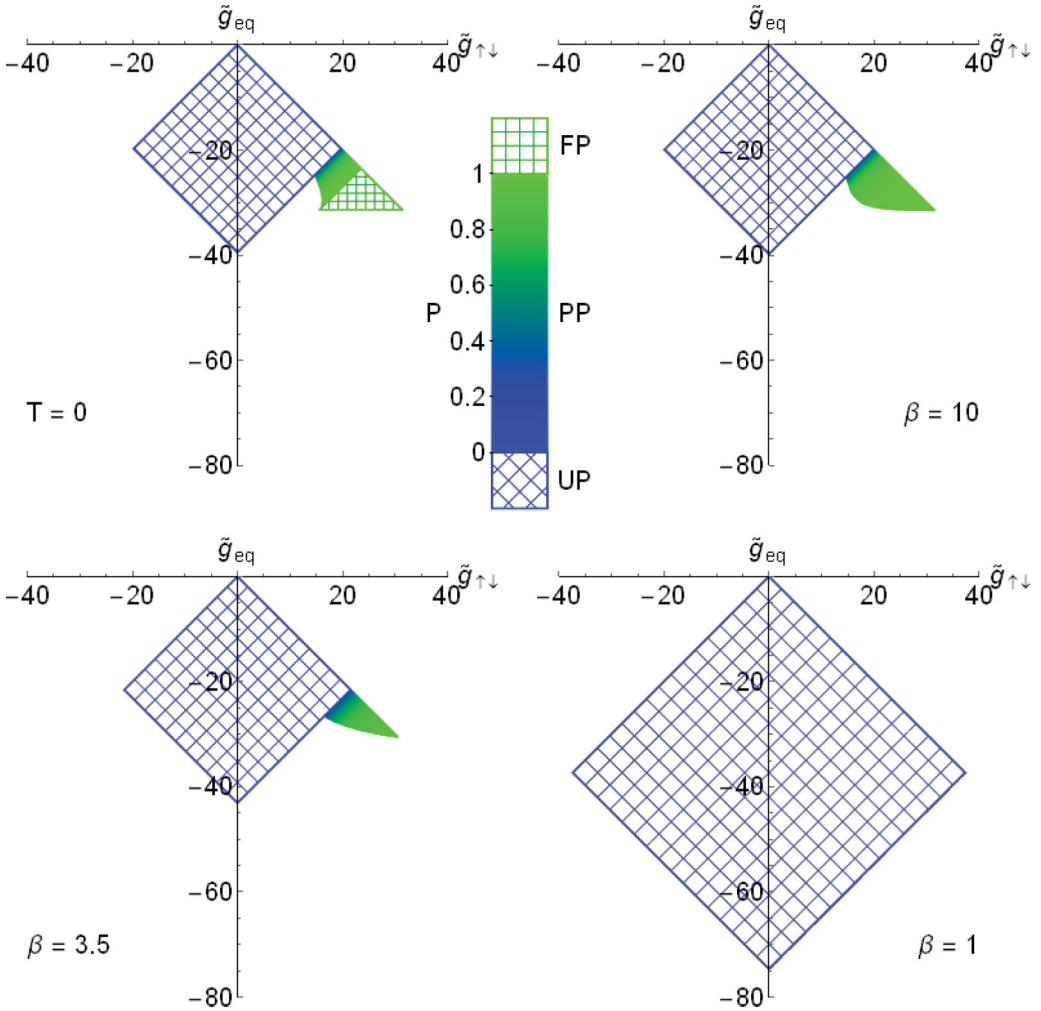

FIG. 5. The regions where the Hessian matrix at the saddle point is positive are shown as a function of the modified interaction parameters $\tilde{g}_{eq}$ and $\tilde{g}_{\uparrow\downarrow}$ for different values of the inverse temperature: $\beta \to +\infty$ ($T = 0$), $\beta = 10$, $\beta = 3.5$, and $\beta = 1$. The area where the unpolarized (UP) state is the saddle point has blue borders and diagonal blue hatching. The area with green borders and darker green horizontal and vertical hatching shows where the fully polarized (FP) state is the saddle point. Finally, in the colored area the partially polarized (PP) state is the saddle point, and color indicates the polarization.

In our theoretical description, we investigate within the manifold of uniform states whether an extremum of the free energy is a minimum or not. If we were to include the lower branch in the manifold of states, this would give our minimum a pathway to decay into the lower energy branch. In the absence of this pathway, the states that we identify can be called stable. Of course, we agree that this does not imply that such states are always stable in current experiments, where an initially prepared nonequilibrium configuration can be used to probe a much larger manifold of states, including those where there is a decay into the lower branch.

V. DISCUSSION

Whereas the lower critical interaction strength discussed above is suitable to describe the transition between the normal and ferromagnetic states, the upper critical interaction value $k_F a_s = 1.23$ indicates another instability that occurs in our model when $\tilde{g}_{\uparrow\downarrow} = -\tilde{g}_{eq}$. In contrast to our result, current experimental data suggests a continuation of the ferromagnetic phase beyond $k_F a_s = 1.23$. Notice that the experimental setup starts from a two-domain magnetic phase out of equilibrium, from which spin diffusion across the domain boundary is measured as the system relaxes towards equilibrium. This situation is different from the one we model: within the manifold of states described by the density fields introduced in the Hartree channel, the present method only investigates uniform densities and equilibrium physics. Since no stable saddle-point solution with such a uniform density exists, this indicates that the true minimum within this particular manifold corresponds to a nonuniform state. Hence, if ferromagnetism survives beyond the region where the uniform saddle point is stable, this suggests that multidomain configurations may be more stable than single-domain states for large values of $k_F a_s$.

A simplified argument showing that an increase of $k_F a_s$ leads to the appearance of nonuniform states can be formulated as follows. The polarization $P = (N_\uparrow - N_\downarrow)/(N_\uparrow + N_\downarrow)$ is a function of temperature, and for any nonzero temperature $|P| < 1$. In the uniform state, the spin-up and spin-down clouds interpenetrate by definition and fill the entire volume V of a

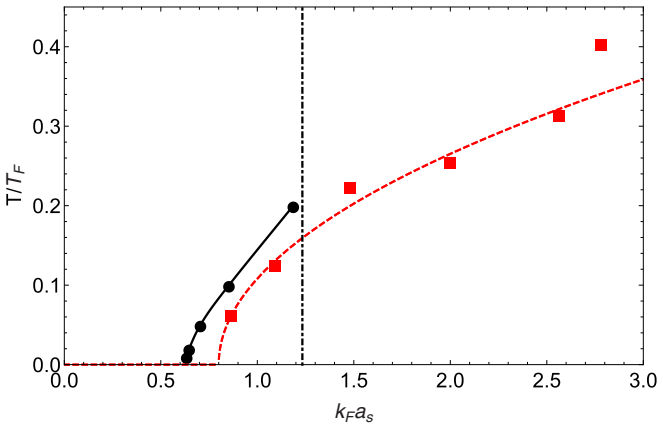

FIG. 6. The critical temperature for itinerant ferromagnetism is plotted as a function of $k_F a_s$ (where a_s is the scattering length determining the dimensionless parameter $\tilde{g}_{\uparrow\downarrow}$, from Fig. 5). The red squares are experimental results from Valtolina *et al.*, Ref. [35]. The red dashed curve is the result of a fit of a square-root power law to the experimental data, also from [35]. The black dots joined by the black curve are the result from the present theory for a fixed value of the (unknown) Fock contribution strength ($\tilde{g}_{\rm eq} = -31$). The black dash-dotted line indicates the value of $k_F a_s$ above which the single-domain, uniform saddle point is unstable.

box. For a fixed number of particles N and fixed polarization P, the ground-state energy of the system is

$$\frac{E}{(3/5)NE_F} = \frac{1}{2}[(1+P)^{5/3} + (1-P)^{5/3}] - \alpha(1+P^2) + \gamma(1-P^2), \tag{30}$$

where $E_F = (\hbar^2/2m)(3\pi^2 N/V)^{2/3}$ is the Fermi energy, and

$$\alpha = \frac{5}{(6\pi)^2}(8\pi k_F |a_{\rm eq}|), \tag{31}$$

$$\gamma = \frac{5}{(6\pi)^2}(8\pi k_F a_{\uparrow\downarrow}), \tag{32}$$

are the ratios between the interaction energies at $P = 0$ and the kinetic energy at $P = 0$. The parameter α describes the equal-spin interactions with $a_{\rm eq} = a_p/r_p^2$, where a_p is the p-wave scattering volume and r_p is the spatial interaction range. The parameter γ describes the opposite-spin interaction with $a_{\uparrow\downarrow} = a_s$, where a_s is the s-wave scattering length. The kinetic energy [first term in Eq. (30)] favors states where both spins can coexist with zero polarization. Both interaction energies [second and third terms in Eq. (30)] favor states with larger polarization. However, for any given polarization P, the equal-spin interaction lowers the energy (equal spins attract), whereas the opposite-spin interaction *increases* the energy (opposite spins repel).

Now consider a nonuniform state with the same N and P values but which is completely phase separated. The total volume remains equal to that of the uniform state, so each spin species occupies one half of the volume. The energy becomes

$$\frac{E}{(3/5)NE_F} = (1+P)^{5/3} + (1-P)^{5/3} - 2\alpha(1+P^2). \tag{33}$$

The first term (the kinetic energy) and the second term (the equal-spin interaction energy) remain present and double in value, but the opposite-spin interaction energy vanishes. Since in Eq. (33) the energy is independent of γ, whereas in Eq. (30) the energy grows linearly with γ, this means that there exists a critical value $\gamma_{\rm cr}$ such that the nonuniform state is lower in energy. In the argument above, we compared two simple situations which did not include effects such as domain wall structure. Therefore, the exact result for the critical value $\gamma_{\rm cr}$ cannot be found from this simple argument; however, it is clear that such a critical value must exist. The inclusion of more detailed structure in variational spin density profiles would only reduce the energy in Eq. (33), leading to a smaller value of $\gamma_{\rm cr}$. The adaptation of the current formalism to nonuniform itinerant ferromagnetic phases, including in particular domain wall physics, is left for future analysis.

The itinerant ferromagnetic phase is predicted in regimes where the interaction energy is comparable to the kinetic energy, and hence competing strongly correlated phases need to be discussed. We begin our discussion by reminding the reader that the issue of itinerant ferromagnetism in the context of ultracold quantum gases is different from that found for electrons in metals. The existence of possible competing phases depends strongly on the interaction form (range, strength, anisotropy, etc.) and on whether the fermions are charged or neutral. Next, let us highlight and contrast some of these phases.

One of the major differences is that in a dilute isotropic 3D quantum gas with short-ranged repulsive interactions, even when the interaction energy dominates the kinetic energy, Wigner crystallization does not occur, while for charged particles this phase is expected theoretically in the low-density regime and has been experimentally observed.

Another possibility, already mentioned above, is a competing phase involving spin or charge-density waves. As we discussed, we do not expect the CDW and SDW instabilities to occur here, since in 3D systems with spherical Fermi surfaces nesting is suppressed [7].

A p-wave superfluid phase can exist in the absence of repulsive s-wave interactions, but the p-wave interaction strengths considered here are approximately $k_F^3 a_p \approx 10^{-4}$ for an interaction range in real space given by $k_F r_p \approx 10^{-2}$. For a fixed interaction range, this leads to a critical temperature [55] that is exponentially small, $T_c \propto T_F \exp\{-\pi/(k_F^3|a_p|)\}$, and hence much lower than the temperatures that can be achieved experimentally. In addition, the inclusion of s-wave repulsive interactions tends to suppress the p-wave superfluid state, even at these very low temperatures.

Therefore we are left with the possibility of phase separation and domain formation whenever the uniform ferromagnetic state is no longer a minimum of the free energy.

VI. CONCLUSION

In this paper, we have shown that itinerant ferromagnetism for atomic Fermi gases is different from that of electron gases in metals due to the short-range nature of atomic interactions. We have demonstrated that the Pauli exclusion principle may be violated when performing a naive saddle-point approximation to the effective action resulting from the Hubbard-Stratonovich transformation in the Hartree channel. As a remedy, we have proposed to use a modified density-density pseudopotential

that correctly describes both the local (Hartree) and the nonlocal (Fock) terms and preserves the Pauli exclusion principle.

Furthermore, we demonstrated that this approach leads to a good saddle-point description of the ferromagnetic transition. We studied the existence-stability region for the saddle points in the plane of equal- versus opposite-spin interaction strengths. Lastly, we obtained the critical temperature for itinerant ferromagnetism as a function of the interaction parameter $k_F a_s$ and compared it with the results of a recent experiment [35]. Our analysis was performed for single-domain, uniform ferromagnetic phases, which become unstable for larger values of the opposite-spin scattering parameter, possibly leading to a nonuniform itinerant ferromagnetic state.

ACKNOWLEDGMENTS

The authors would like to thank F. Brosens, W. Ketterle, G. M. Bruun, and A. Pelster for interesting discussions, and J. P. A. Devreese for a careful reading of the manuscript. E.V. gratefully acknowledges support in the form of a Ph.D. fellowship of the Research Foundation – Flanders (FWO). This work was supported by the following Research Projects of the Research Foundation – Flanders (FWO): G.0119.12N, G.0122.12N, G.0429.15N, and WOG (WO.035.04N). The work was also supported by the Research Fund of the University of Antwerp (J.T.) and the Army Research Office (ARO) (Grant No. W911NF-09-1-0220) (C.A.R.S.dM).

[1] F. Bloch, Z. Phys. **57**, 545 (1929).
[2] W. Heisenberg, Z. Phys. **49**, 619 (1928).
[3] E. C. Stoner, Philos. Mag. **15**, 1018 (1933).
[4] E. P. Wigner, Phys. Rev. **46**, 1002 (1934); Trans. Faraday Soc. **34**, 678 (1938).
[5] D. M. Ceperley and B. J. Alder, Phys. Rev. Lett. **45**, 566 (1980).
[6] A. W. Overhauser, Phys. Rev. **167**, 691 (1968).
[7] T. M. Rice, Phys. Rev. B **2**, 3619 (1970).
[8] M. Houbiers, R. Ferwerda, H. T. C. Stoof, W. I. McAlexander, C. A. Sackett, and R. G. Hulet, Phys. Rev. A **56**, 4864 (1997).
[9] M. Amoruso, I. Meccoli, A. Minguzzi, and M. P. Tosi, Eur. Phys. J. D **8**, 361 (2000).
[10] L. Salasnich, B. Pozzi, A. Parola, and L. Reatto, J. Phys. B **33**, 3943 (2000).
[11] T. Sogo and H. Yabu, Phys. Rev. A **66**, 043611 (2002).
[12] R. A. Duine and A. H. MacDonald, Phys. Rev. Lett. **95**, 230403 (2005).
[13] G.-B. Jo, Y.-R. Lee, J.-H. Choi, C. A. Christensen, T. H. Kim, J. H. Thywissen, D. E. Pritchard, and W. Ketterle, Science **325**, 1521 (2009).
[14] G. J. Conduit and B. D. Simons, Phys. Rev. Lett. **103**, 200403 (2009).
[15] A. Recati and S. Stringari, Phys. Rev. Lett. **106**, 080402 (2011).
[16] C. Sanner, E. J. Su, W. Huang, A. Keshet, J. Gillen, and W. Ketterle, Phys. Rev. Lett. **108**, 240404 (2012).
[17] S. Zhang and T.-L. Ho, New J. Phys. **13**, 055003 (2011).
[18] D. Pekker, M. Babadi, R. Sensarma, N. Zinner, L. Pollet, M. W. Zwierlein, and E. Demler, Phys. Rev. Lett. **106**, 050402 (2011).
[19] I. Berdnikov, P. Coleman, and S. H. Simon, Phys. Rev. B **79**, 224403 (2009).
[20] S. Zhang, H.-H. Hung, and C. Wu, Phys. Rev. A **82**, 053618 (2010).
[21] S. K. Baur and N. R. Cooper, Phys. Rev. Lett. **109**, 265301 (2012).
[22] P. Massignan, Z. H. Yu, and G. M. Bruun, Phys. Rev. Lett. **110**, 230401 (2013).
[23] Y. Z. Jiang, D. V. Kurlov, X. W. Guan, F. Schreck, and G. V. Shlyapnikov, Phys. Rev. A **94**, 011601 (2016).
[24] C. Kohstall, M. Zaccanti, M. Jag, A. Trenkwalder, P. Massignan, G. M. Bruun, F. Shreck, and R. Grimm, Nature (London) **485**, 615 (2012).
[25] A. Ambrosetti, G. Lombardi, L. Salasnich, P. L. Silvestrelli, and F. Toigo, Phys. Rev. A **90**, 043614 (2014); A. Ambrosetti, P. L. Silvestrelli, F. Pederiva, L. Mitas, and F. Toigo, *ibid.* **91**, 053622 (2015).
[26] X. Cui and T.-L. Ho, Phys. Rev. A **89**, 023611 (2014).
[27] E. J. Lindgren, J. Rotureau, C. Forssén, A. G. Volosniev, and N. T. Zinner, New J. Phys. **16**, 063003 (2014).
[28] S. Pilati, I. Zintchenko, and M. Troyer, Phys. Rev. Lett. **112**, 015301 (2014).
[29] I. Zintchenko, L. Wang, and M. Troyer, Eur. Phys. J. B **89**, 180 (2016).
[30] E. Vermeyen and J. Tempere, J. Low Temp. Phys. **179**, 175 (2015).
[31] M. Barth and W. Zwerger, Ann. Phys. **326**, 2544 (2011).
[32] P. Massignan, M. Zaccanti, and G. M. Bruun, Rep. Prog. Phys. **77**, 034401 (2014).
[33] R. Roth and H. Feldmeier, J. Phys. B **34**, 4629 (2001).
[34] X. Cui and H. Zhai, Phys. Rev. A **81**, 041602(R) (2010).
[35] G. Valtolina, F. Scazza, A. Amico, A. Burchianti, A. Recati, T. Enss, M. Inguscio, M. Zaccanti, and G. Roati, Nat. Phys. **13**, 704 (2017).
[36] K.-K. Ni, S. Ospelkaus, D. Wang, G. Quéméner, B. Neyenhuis, M. H. G. de Miranda, J. L. Bohn, J. Ye, and D. S. Jin, Nature (London) **464**, 1324 (2010).
[37] M. Lu, N. Q. Burdick, and B. L. Lev, Phys. Rev. Lett. **108**, 215301 (2012).
[38] K. Aikawa, A. Frisch, M. Mark, S. Baier, R. Grimm, and F. Ferlaino, Phys. Rev. Lett. **112**, 010404 (2014).
[39] S. D. Mahanti and S. S. Jha, Phys. Rev. E **76**, 062101 (2007).
[40] T. Miyakawa, T. Sogo, and H. Pu, Phys. Rev. A **77**, 061603(R) (2008).
[41] B. M. Fregoso and E. Fradkin, Phys. Rev. Lett. **103**, 205301 (2009).
[42] N. D. Drummond, N. R. Cooper, R. J. Needs, and G. V. Shlyapnikov, Phys. Rev. B **83**, 195429 (2011).
[43] C. Chin, R. Grimm, P. Julienne, and E. Tiesinga, Rev. Mod. Phys. **82**, 1225 (2010).
[44] L. Yang, X. Guan, and X. Cui, Phys. Rev. A **93**, 051605(R) (2016).
[45] H. Matsumoto, H. Umezawa, S. Seki, and M. Tachiki, Phys. Rev. B **17**, 2276 (1978).
[46] S. Seki, H. Matsumoto, M. Tachiki, and H. Umezawa, Prog. Theor. Phys. **61**, 1034 (1979).

[47] E. Kolley and W. Kolley, Phys. Status Solidi B **105**, K85 (1981).
[48] H. Kleinert, *Path Integrals in Quantum Mechanics, Statistics, Polymer Physics, and Financial Markets*, 5th ed. (World Scientific, Singapore, 2009).
[49] N. Nagaosa, *Quantum Field Theory in Condensed Matter Physics* (Springer, Berlin, 2010).
[50] J. Whitehead, H. Matsumoto, and H. Umezawa, Phys. Rev. B **25**, 4737 (1982).
[51] H. Kleinert, Elect. J. Theor. Phys. **8**, 57 (2011).
[52] H. Kleinert, Phys. Lett. B **434**, 74 (1998).
[53] H. Park, K. Haule, C. A. Marianetti, and G. Kotliar, Phys. Rev. B **77**, 035107 (2008).
[54] S. Pilati, G. Bertaina, S. Giorgini, and M. Troyer, Phys. Rev. Lett. **105**, 030405 (2010).
[55] M. Iskin and C. A. R. Sa de Melo, Phys. Rev. Lett. **96**, 040402 (2006).